Active vibration control with a combination of virtual controlled object-based model-free design and fuzzy sliding mode technique

Heisei Yonezawa#1, Ansei Yonezawa#2, Itsuro Kajiwara#3

#1(Corresponding author)
Division of Mechanical and Aerospace Engineering, Hokkaido University
N13, W8, Kita-ku, Sapporo, Hokkaido 060-8628, Japan
Phone +81-80-4039-9406
E-mail: yonezawah@eng.hokudai.ac.jp
ORCID: 0000-0001-9808-2224

#2
Division of Mechanical and Aerospace Engineering, Hokkaido University
N13, W8, Kita-ku, Sapporo, Hokkaido 060-8628, Japan
Phone +81- 90-2893-3160
E-mail: 0316ansei@gmail.com
ORCID: 0000-0001-5077-5259

#3
Division of Mechanical and Aerospace Engineering, Hokkaido University
N13, W8, Kita-ku, Sapporo, Hokkaido 060-8628, Japan
Phone +81-11-706-6390, Fax. +81-11-706-6390
E-mail: ikajiwara@eng.hokudai.ac.jp
ORCID: 0000-0003-2651-7289

Abstract

[Purpose]

Active vibration control typically requires mathematical modeling of the plant, which increases development costs and burdens for designers. This study develops a novel model-free vibration controller that can be designed without using any models or parameters of a real controlled object.

[Methods]

This study proposes a new model-free fuzzy sliding mode vibration controller based on a virtual controlled object (VCO). The key idea is the combination of the VCO-based model-free controller design, sliding mode control (SMC), and fuzzy adaptive compensation for chattering elimination. By inserting the VCO, defined as a single-degree-of-freedom (SDOF) structure, between a real controlled object and an actuator, the model-free control system is realized. According to a simple inequality-based condition, the VCO parameters are specified to enable the design of an active vibration controller without requiring any models or parameters of the controlled object. This design scheme is directly applied to the sliding mode control theory, and convergence is analyzed using a Lyapunov function technique. To eliminate the chattering phenomenon, a fuzzy-inference-based compensation is introduced. Considering variations in the switching function, this fuzzy inference modifies the nonlinear switching input online to prevent chattering while ensuring the state trajectory rapidly converge to the sliding surface.

[Results]

Simulation verifications are conducted with various mechanical structures, including time-varying system. The present approach achieves good vibration control performance without causing the chattering phenomenon. Comparative study reveals the advantage of the present approach over the conventional model-based controller design from the viewpoint of its simple design procedure and robustness.

[Conclusion]

The proposed model-free fuzzy SMC provides sufficient damping performance and excellent robustness, showing its practical usability.

Keywords: Model-free control, Active vibration control, Virtual controlled object, Sliding mode control, Proof-mass actuator, Fuzzy logic

1. Introduction

Vibrations hinder improvements in the comfort and precision of mechanical systems and cause fatigue failures and noise problems [1]. Therefore, vibration control is regarded as a core technology required for improving the performance of mechanical systems [2][3][4]. The growing popularity of flexible structures and the recent trend toward smaller, lighter machines underscore the significance of this technology [5][6]. Active vibration control, in particular, has attracted a great deal of attention due to its potential to provide powerful vibration suppression effects for intricate systems [7][8][9].

Active vibration control is generally model-based, meaning the control system design requires mathematical modeling of real controlled structures via experimental modal analysis, finite element methods, etc. The need for such modeling processes increases development costs and burdens for designers. Additionally, a model-based controller is susceptible to characteristic changes that always exist in real mechanical systems. The controller's dependence on a specific structure (accurate modeling) hinders the application of the same controller to various other systems.

To avoid the mathematical modeling of controlled objects, many previous works have developed model-free controls (MFC). One efficacious strategy is to employ artificial intelligence, such as neural networks (NN) [10][11][12]. A representative method involves identifying an inverse plant model using an artificial neural network, leading to the direct inverse controller [13]. The nonlinear autoregressive with exogenous input neural network has been used to identify a dynamic model [14]. The applications of radial basis function NNs have been increasing in advanced vibration controls [15][16]. However, collecting a huge amount of training data and undergoing the training process are necessary to attain suitable control behavior. This requirement imposes significant design costs on most NN-based approaches.

Direct data-driven approaches use a systematic controller design method that relies on the input and output data of a plant instead of accurate mathematical modeling. This approach also enables MFC. Notable methods, such as virtual reference feedback tuning [17][18] and fictitious reference iterative tuning [19][20], have been established with a wide variety of industrial applications [21]. Inspired by this basic idea, numerous efforts have recently been dedicated to developing extended versions [22][23]. However, these approaches require high-quality data, as the success of the controller design, including numerical stability, largely depends on the quality of the acquired data. It should be noted that collecting such high-quality data is not easy.

Consequently, there has been no attempt to develop a simple and practical model-free active damping controller. Recently, motivated by this background, a new model-free active vibration suppression strategy has been proposed based on the concept of a virtual controlled object (VCO) [24], namely VCO-based model-free control (VCO-MFC). This approach allows for the design of a vibration controller based on a system composed only of the VCO and an actuator, rather than the actual controlled object, resulting in a model-free design. Despite the simplicity of deriving a model-free controller by simply introducing the VCO, the excellent robustness has been experimentally confirmed for changing controlled structures [25][26][27]. Several experimental studies have demonstrated that VCO-MFC can successfully attenuate the vibration occurring at continuous structures without spillover [27][28]. One of the notable benefits of this approach is that the design procedure after incorporating the VCO is exactly the same as that of mature model-based control theories. This means that we can directly apply various model-based control designs.

Nonlinear control theory is also applicable to the VCO-based approach. Sliding mode control (SMC) is a representative nonlinear robust control theory characterized by the switching of the control input according to changes in the plant state. The remarkable feature of SMC is its robustness against plant uncertainties and disturbances. Due to the extendibility of VCO-MFC, combining it with SMC can further enhance robustness to plant variations [29]. In many previous works, the robustness of SMC has been demonstrated for uncertain systems [30]. In the context of VCO-MFC, a previous study has revealed that the uncertainty of the model parameter of the actuator satisfies the so-called matching condition [29]. Then, the study [29] has examined the VCO-based SMC technique with the robustness to the actuator uncertainty, since SMC is insensitive to the matched uncertainties and disturbances [31]. The combination with NNs is also effective in dealing with unknown system dynamics and nonlinearities [32][33]. The role of such NNs is primarily to estimate the uncertain models. As a suitable application, various types of SMC have been examined for active suspension systems [34], exploring several unique techniques such as disturbance observer-based SMCs [35][36] and a time-delay estimation-based approach [37]. Other vibration control applications cover interarea oscillations for doubly fed induction generators [38], chatter vibration in milling processes [39], and soft robots [40].

Nevertheless, most existing SMCs depend on models or parameters of the controlled plants in the design process. Some model-free approaches exist [41][42][43]; however, remaining issues may deteriorate practicability, such as sophisticated design schemes with many processes and adjustable variables, insufficient consideration for chattering, and the need for an estimator for unknown system dynamics.

To compensate for the disadvantages of existing SMCs, a fuzzy SMC (FSMC) has been employed as one of the promising choices. Originating from the capability of fuzzy logic to grant adaptability and robustness to controllers, the natural extension is its combination with SMC. Many types of FSMC have been examined for various mechanical systems [44][45], including vibration suppression for structures. Based on a bioinspired reference model, an adaptive FSMC considering the input effects of dead zone and saturation has been developed for vehicle active suspension systems [46]. Other examples of FSMCs for suspension systems can also be found [47]. A Takagi-Sugeno (T-S) fuzzy method is applicable to construct FSMCs to handle plant nonlinearities and uncertainties [48][49]. To suppress earthquake-induced vibrations in building structures, a variable fractional-order SMC has been improved with a fuzzy-logic-based adaptive approximation approach [50]. A fuzzy fast terminal SMC has been utilized for active damping of a two-connected flexible piezoelectric plate [51]. Numerous works have suggested that the use of fuzzy logic enables mitigating the chattering effects [52].

However, most of the existing FSMCs require models or parameters of the controlled objects, as well as information on the uncertainty in their design process, increasing the associated costs and burdens. Furthermore, the design process is also complicated, involving the necessity of adaptive estimation/approximation mechanisms [53] or training processes [54].

Motivated by the gaps in the existing literatures, this study proposes a new fuzzy SMC, namely, VCO-based model-free fuzzy SMC (VCO-MFFSMC), to simplify the model-free design for structural vibration controls. The key idea is the combination of the VCO-based model-free design, an SMC technique, and fuzzy adaptive compensation to reduce chattering. First, the VCO, defined as a single degree-of-freedom (SDOF) system, is introduced between a real controlled structure and an actuator. A simple inequality-based condition specifies the suitable parameters for the VCO. Then, a well-established SMC design scheme is directly applied to the system composed only of the VCO and the actuator instead of the real controlled object, presenting the model-free SMC. The convergence of the SMC is guaranteed based on a Lyapunov function technique. Additionally, the fuzzy adaptive compensation is introduced to reduce the chattering phenomenon. This fuzzy inference adaptively modifies the nonlinear switching input without inducing chattering, ensuring that the state trajectory rapidly converges to the sliding surface. Finally, the proposed approach is verified through applications to various structural vibration problems. In contrast to a previous related study [55], more detailed analysis is performed via numerical examples involving a time-varying system and comparison with a model-based controller.

The contributions and technical novelties of this study are summarized as follows.

(1) This study proposes a novel model-free fuzzy sliding mode vibration controller that can be designed without using any models and parameters of a real controlled object at all.

(2) Compared with existing FSMCs, the proposed VCO-MFFSMC has a simpler design process and is easy to implement. This is because the model-free design is allowed by simply setting the VCO, which is defined as a simple SDOF and can be specified according to a controlled frequency band-based inequality condition.

(3) Compared with the previous work [29], the introduction of adaptive fuzzy inference makes the proposed SMC free from severe chattering, which has been a barrier against successful implementations of SMCs.

(4) Comparative study reveals the advantage of the present approach over the conventional model-based controller design from the viewpoint of its simple design procedure and robustness to characteristic changes in an actual controlled object.

The remainder of this paper is organized as follows. Section 2 describes the basic concept of the VCO-based model-free active vibration control strategy. Section 3 provides the design procedure of the VCO-based model-free sliding mode controller. The chattering compensation strategy based on the fuzzy logic is proposed in Section 4. Section 5 demonstrates the validity of the proposed control scheme through vibration control simulations. Finally, Section 6 concludes the paper.

2. Model-free vibration control strategy based on VCO (VCO-MFC)

This study employs the electromagnetic proof-mass actuator, as shown in Fig. 1. Due to its mechanical principle, the actuator model has been established as an SDOF system [24].

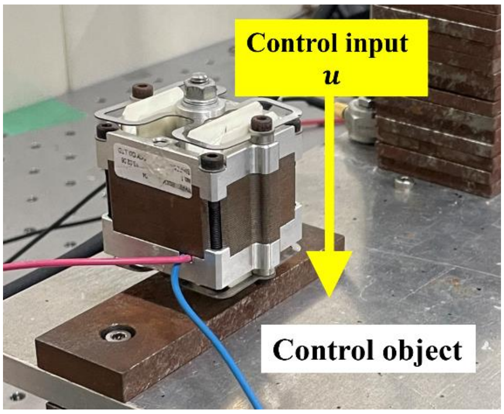

Fig. 1: Proof-mass actuator.

The proposed method realizes a model-free design of a vibration suppression controller by intercalating the SDOF VCO between the actual controlled object and the actuator [24]. First, we consider an actual mechanical configuration to perform vibration control, as shown in Fig. 2(a). The symbols m_a, k_a, and c_a indicate the mass, stiffness, and damping of the actuator, respectively. The actual controlled structure is assumed to be arbitrary. The aim of the system in Fig. 2(a) is to damp displacement oscillation x_1 of the actual controlled object via the control input u generated by the actuator.

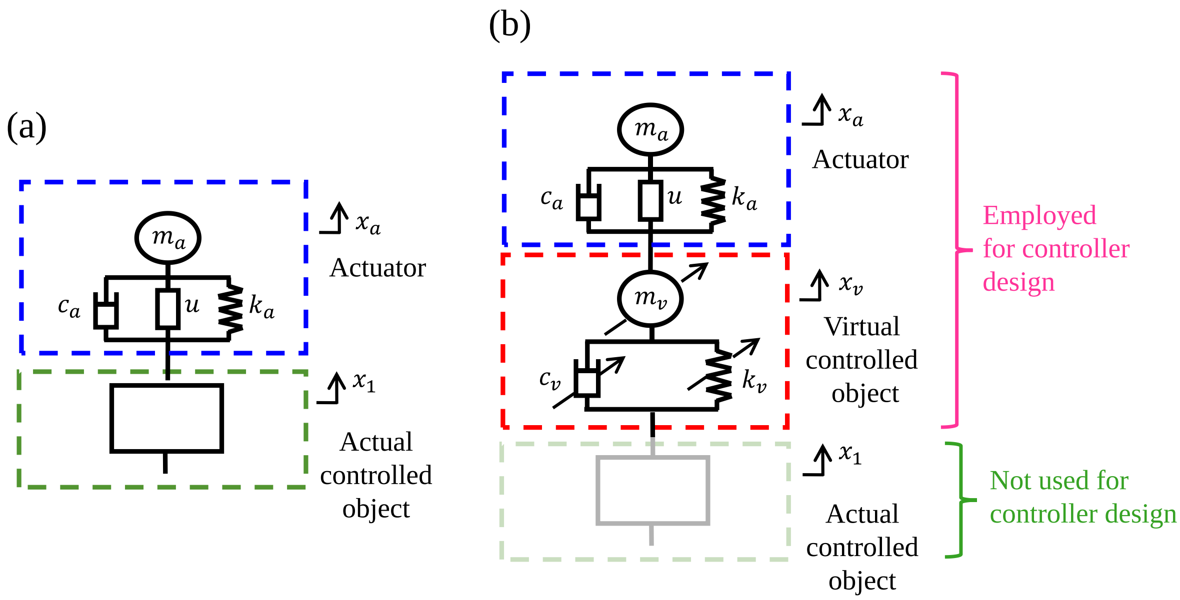

Fig. 2: VCO-based model-free controller design: (a) real control system and (b) system with VCO.

Figure 2 (b) shows the system used for model-free controller design. We can see that the VCO is newly introduced between the real controlled object and the actuator. The fundamental concept of the VCO-MFC design is that a vibration controller is designed using the 2DOF system consisting only of the actuator and the VCO instead of the model including the real controlled object. In other words, this approach regards the VCO as a temporary controlled object instead of the actual controlled object, and the designed controller to suppress x_v (vibration of the VCO) indirectly suppresses x_1 (vibration of the actual object) as well. As discussed later, the parameters of the VCO (i.e., mass m_v, spring constant k_v, and damper c_v) are design variables. After setting of the VCO, a model-free vibration controller is easily obtained because the subsequent design process applied for the VCO-actuator 2DOF system is the same as that of matured model-based control theories. The equations of motion for the VCO and the actuator in Fig. 2(b) can be derived as follows:

$$m_a \ddot{x}_a = u - k_a(x_a - x_v) - c_a(\dot{x}_a - \dot{x}_v) \tag{1}$$

$$m_v \ddot{x}_v = -u - k_a(x_v - x_a) - c_a(\dot{x}_v - \dot{x}_a) - k_v(x_v - x_1) - c_v(\dot{x}_v - \dot{x}_1) \tag{2}$$

Applying Laplace transformation to Eqs. (1) and (2) gives the transfer function T_{xvx1} from x_1 to x_v as follows:

$$\begin{aligned} T_{xvx1} &= \frac{\hat{x}_v(s)}{\hat{x}_1(s)} \\ &= \frac{(c_v s + k_v)(m_a s^2 + k_a + c_a s)}{-(c_a s + k_a)^2 + (m_a s^2 + c_a s + k_a)\{m_v s^2 + (k_a + k_v) + (c_a + c_v)s\}} \end{aligned} \tag{3}$$

In Eq. (3), s indicates the Laplace operator. A Laplace transform for a time-domain function $f(t)$ is denoted as $\hat{f}(\mathrm{s})$.

Regarding T_{xvx1}, satisfying the condition $T_{xvx1} \approx 1$ in the controlled frequency band means that $x_v \approx x_1$ holds in the controlled frequency band. Under $T_{xvx1} \approx 1$, the indirect vibration control of x_1 can be established by suppressing x_v. Therefore, the VCO parameters should be set to satisfy $T_{xvx1} \approx 1$ in the controlled frequency band. The previous work [24] has derived a quantitative design condition as the following inequality:

$$\frac{1}{m_v}\left\{(\Omega_k^{cont})^2 + k_v\left(-\frac{1}{m_a} + \frac{(\Omega_k^{cont})^2}{k_a}\right)\right\} > (\Omega_k^{cont})^2\left(-\frac{1}{m_a} + \frac{(\Omega_k^{cont})^2}{k_a}\right), (k = 1, 2) \tag{4}$$

For realizing model-free control, the values of k_v and m_v should satisfy Eq. (4). Previous work [24] has shown that satisfying the condition (4) with the proper values of k_v and m_v results in $T_{xvx1} \approx 1$ (i.e., $x_v \approx x_1$) in the controlled frequency band. The symbols Ω_1^{cont} and Ω_2^{cont} ($\Omega_2^{cont} > \Omega_1^{cont} \geq \sqrt{k_0/m_0}$) represent the lower and the upper bound frequencies of the controlled frequency band, respectively. Qualitatively, $T_{xvx1} \approx 1$ can be achieved by setting m_v and k_v as sufficiently small and sufficiently large values, respectively, to avoid that the VCO has the resonant peak in the controlled frequency band. The remarkable point is that Eqs. (3) and (4) contain no models or parameters of real controlled objects at all. Because the design condition (4) depends only on the controlled frequency band (Ω_1^{cont} and Ω_2^{cont}) and the actuator specifications, the VCO can be specified irrespective of actual plant characteristics. Note that the VCO is not the reduced-order model of the actual controlled object. Table 1 lists the specifications in this study. In this study, the controlled frequency band lies in $f \in (\Omega_1^{cont} = 5.0 \times 10^1$ Hz$, \Omega_2^{cont} = 3.0 \times 10^3$ Hz). Figure 3 describes the Bode diagram of $T_{xvx1}(j\omega)$. Within the controlled frequency band, the required characteristic where the gain is almost 1.0 and the phase is regarded as 0 degrees is achieved.

Table 1. Parameters for the model-free control system design.

Properties	Value	Unit
m_a	0.2013	kg
k_a	3518	N/m
c_a	1.186	Ns/m
m_v	1.0×10^{-5}	kg
k_v	7.0×10^{5}	N/m
c_v	0.0	Ns/m

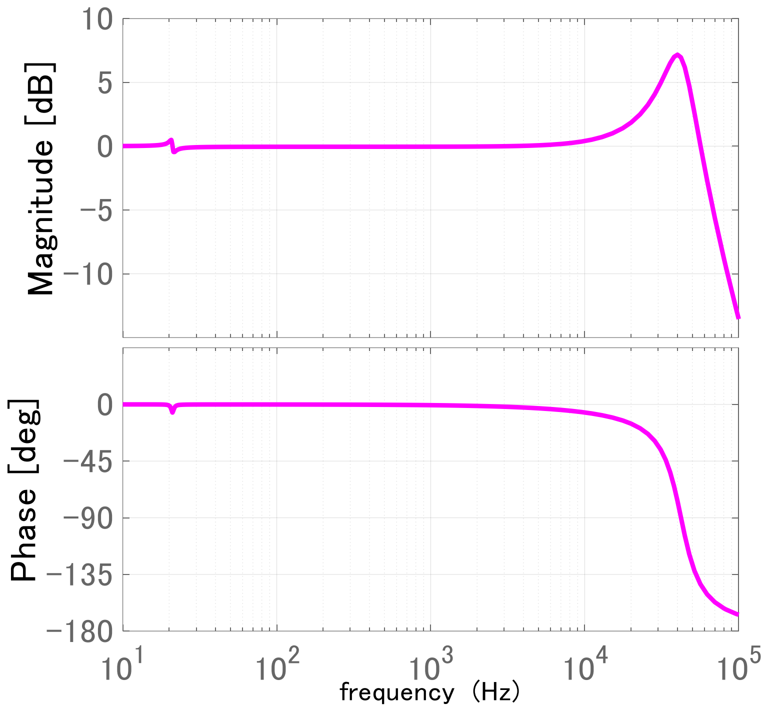

Fig. 3: Transfer characteristic from vibration of the actual controlled object to that of VCO.

To design a model-free controller for the 2DOF system in Fig. 2(b), the state equation needs to be derived. For Eqs. (1) and (2), $w \in \mathbb{R}$ is defined as the disturbance, which originates from the vibration of the actual controlled object, as shown in Eq. (5).

$$w = c_v \dot{x}_1 + k_v x_1 \tag{5}$$

Eqs. (6)–(14) show the state space representation.

$$\dot{\boldsymbol{x}}_{MF} = \boldsymbol{A}_{MF}\boldsymbol{x}_{MF} + \boldsymbol{B}_{MF1}w + \boldsymbol{B}_{MF2}u \tag{6}$$

$$\boldsymbol{y}_{MF} = \boldsymbol{C}_{MF}\boldsymbol{x}_{MF} + D_{MF1}w + D_{MF2}u \tag{7}$$

$$\boldsymbol{x}_{MF} = [x_v \quad x_a \quad \dot{x}_v \quad \dot{x}_a]^T \tag{8}$$

$$\boldsymbol{A}_{MF}=\begin{bmatrix} 0 & 0 & 1 & 0 \\ 0 & 0 & 0 & 1 \\ -\frac{k_a+k_v}{m_v} & \frac{k_a}{m_v} & -\frac{c_a+c_v}{m_v} & \frac{c_a}{m_v} \\ \frac{k_a}{m_a} & -\frac{k_a}{m_a} & \frac{c_a}{m_a} & -\frac{c_a}{m_a} \end{bmatrix} \tag{9}$$

$$\boldsymbol{B}_{MF1}=\begin{bmatrix} 0 & 0 & \frac{1}{m_v} & 0 \end{bmatrix}^T \tag{10}$$

$$\boldsymbol{B}_{MF2}=\begin{bmatrix} 0 & 0 & -\frac{1}{m_v} & \frac{1}{m_a} \end{bmatrix}^T \tag{11}$$

$$\boldsymbol{C}_{MF}=\begin{bmatrix} -\frac{k_a+k_v}{m_v} & \frac{k_a}{m_v} & -\frac{c_a+c_v}{m_v} & \frac{c_a}{m_v} \end{bmatrix} \tag{12}$$

$$D_{MF1}=\frac{1}{m_v} \tag{13}$$

$$D_{MF2}=-\frac{1}{m_v} \tag{14}$$

Eqs. (9)–(11) characterize the dynamics of the state of the two-degree-of-freedom (2DOF) system composed of the actuator and the VCO described in Fig. 2(b): the matrix $\boldsymbol{A}_{MF}$ specifies the time evolution of the state $\boldsymbol{x}_{MF}$, whereas $\boldsymbol{B}_{MF1}$ in Eq. (10) and $\boldsymbol{B}_{MF2}$ in Eq. (11) define the effects of the external disturbance w and the control input force u to the state $\boldsymbol{x}_{MF}$, respectively. Therefore, Eqs. (9)–(11) regulate the time evolution of the displacements and velocities of the point mass of the actuator and the VCO.

Eqs. (12)–(14) specify the observed variable of the 2DOF system. In particular, $\boldsymbol{C}_{MF}$, D_{MF1}, and D_{MF2} in Eqs. (12)–(14) indicate that the acceleration $\ddot{x}_v$ of the point mass of the VCO is observed. This is because the acceleration sensor is used to obtain the observed output.

Note that each of the coefficient matrices in Eq. (6) consists only of the VCO and the actuator. That is, this system does not contain any parameters of the real controlled object. Therefore, the direct application of mature model-based control theory to Eq. (6) results in the model-free design of an active vibration controller.

In the dummy-controlled system in Eq. (6), $\ddot{x}_v$ (the vibration of the VCO) is fed back to a model-free vibration controller. In real applications, instead of $\ddot{x}_v$, $\ddot{x}_1$, which is almost equal to $\ddot{x}_v$, is monitored as a measured output since the VCO does not exist in real systems. This measurement is allowed by the establishment of $T_{xvx1} \approx 1$. For multi-degree-of-freedom or continuous structures, a sensor should measure $\ddot{x}_1$ at the location where the actuator is installed.

3. VCO-based model-free SMC

Sliding mode control (SMC) is a type of variable structure control system that discontinuously switches the control inputs depending on changes in the plant's state. The process of designing SMC is divided into two phases: (i) the design of a sliding surface and (ii) the derivation of a nonlinear switching control law. It should be noted that the direct application of this design process to the VCO-based state equation (6) results in a model-free SMC.

3.1. Design of sliding surface

As an ideal system dynamic during sliding mode, a sliding surface $\sigma = 0$ needs to be designed. To minimize the state fluctuations on the sliding surface, a switching function $\sigma \in \mathbb{R}$ is defined as [31]

$$\sigma = \boldsymbol{S}\boldsymbol{x}_{MF} \tag{15}$$

where $\boldsymbol{S} \in \mathbb{R}^{1\times4}$ is a coefficient vector to be designed. Here, we consider the state equation (6) without external disturbances as:

$$\dot{\boldsymbol{x}}_{MF} = \boldsymbol{A}_{MF}\boldsymbol{x}_{MF} + \boldsymbol{B}_{MF2}u \tag{16}$$

$$\boldsymbol{x}_{MF} = [x_v \quad x_a \quad \dot{x}_v \quad \dot{x}_a]^T \tag{17}$$

$$\boldsymbol{A}_{MF} = \begin{bmatrix} 0 & 0 & 1 & 0 \\ 0 & 0 & 0 & 1 \\ -\dfrac{k_a + k_v}{m_v} & \dfrac{k_a}{m_v} & -\dfrac{c_a + c_v}{m_v} & \dfrac{c_a}{m_v} \\ \dfrac{k_a}{m_a} & -\dfrac{k_a}{m_a} & \dfrac{c_a}{m_a} & -\dfrac{c_a}{m_a} \end{bmatrix}$$

$$\boldsymbol{B}_{MF2} = \begin{bmatrix} \boldsymbol{B}_{21} \\ B_{22} \end{bmatrix} = \begin{bmatrix} 0 \\ 0 \\ -\dfrac{1}{m_v} \\ \dfrac{1}{m_a} \end{bmatrix} \tag{18}$$

$$\boldsymbol{B}_{21} = \begin{bmatrix} 0 & 0 & -\dfrac{1}{m_v} \end{bmatrix}^T, B_{22} = \frac{1}{m_a}$$

Applying the variable transformation via a transformation matrix $\boldsymbol{T}_{tr} \in \mathbb{R}^{4\times4}$ results in the following equivalent system.

$$\begin{bmatrix} \dot{\boldsymbol{\xi}}_1 \\ \dot{\xi}_2 \end{bmatrix} = \begin{bmatrix} \boldsymbol{A}_{11} & \boldsymbol{A}_{12} \\ \boldsymbol{A}_{21} & A_{22} \end{bmatrix} \begin{bmatrix} \boldsymbol{\xi}_1 \\ \xi_2 \end{bmatrix} + \begin{bmatrix} 0 \\ B_{22} \end{bmatrix} u \tag{19}$$

$$\begin{bmatrix} \boldsymbol{\xi}_1 \\ \xi_2 \end{bmatrix} = \boldsymbol{T}_{tr}\boldsymbol{x}_{MF} \tag{20}$$

$$\boldsymbol{\xi}_1 \in \mathbb{R}^{3\times1}, \xi_2 \in \mathbb{R}^{1\times1}$$

$$\begin{bmatrix} \boldsymbol{A}_{11} & \boldsymbol{A}_{12} \\ \boldsymbol{A}_{21} & A_{22} \end{bmatrix} = \boldsymbol{T}_{tr}\boldsymbol{A}_{MF}\boldsymbol{T}_{tr}^{-1} \tag{21}$$

$$\boldsymbol{A}_{11} \in \mathbb{R}^{3\times3}, \boldsymbol{A}_{12} \in \mathbb{R}^{3\times1}, \boldsymbol{A}_{21} \in \mathbb{R}^{1\times3}, \boldsymbol{A}_{22} \in \mathbb{R}^{1\times1}$$

$$\boldsymbol{T}_{tr} = \begin{bmatrix} \boldsymbol{I}_{3\times3} & -\boldsymbol{B}_{21}B_{22}^{-1} \\ \boldsymbol{0}_{1\times3} & I_{1\times1} \end{bmatrix} \tag{22}$$

To design the switching function, an optimal control problem is formulated. The quadratic cost function

J_s [31] is defined as Eq. (23), where $\boldsymbol{W}$ is a positive-definite symmetric matrix, and t_s is the time at the moment when the state trajectory reaches the sliding surface. Note that J_s is defined for the system dynamics under the sliding mode. Therefore, J_s does not include the term regarding the control input, since the dynamics under the sliding mode are characterized as the control independent free motion (see Section 2.2 in [31] for the details of the theoretical background).

$$J_s = \int_{t_s}^{\infty} \boldsymbol{x}_{MF}{}^T \boldsymbol{W} \boldsymbol{x}_{MF}\, dt = \int_{t_s}^{\infty} (\boldsymbol{\xi}_1{}^T \widehat{\boldsymbol{q}}_{11} \boldsymbol{\xi}_1 + v^T q_{22} v) dt \tag{23}$$

$$v = \xi_2 + q_{22}{}^{-1} \boldsymbol{q}_{12}{}^T \boldsymbol{\xi}_1 \tag{24}$$

$$\begin{bmatrix} \boldsymbol{q}_{11} & \boldsymbol{q}_{12} \\ \boldsymbol{q}_{21} & q_{22} \end{bmatrix} = \boldsymbol{T}_{tr}{}^T \boldsymbol{W} \boldsymbol{T}_{tr} \tag{25}$$
$$\boldsymbol{q}_{11} \in \mathbb{R}^{3\times3}, \boldsymbol{q}_{12} \in \mathbb{R}^{3\times1}, \boldsymbol{q}_{21} \in \mathbb{R}^{1\times3}, \boldsymbol{q}_{22} \in \mathbb{R}^{1\times1}$$

$$\boldsymbol{q}_{21}{}^T = \boldsymbol{q}_{12} \tag{26}$$

$$\widehat{\boldsymbol{q}}_{11} = \boldsymbol{q}_{11} - \boldsymbol{q}_{12} q_{22}{}^{-1} \boldsymbol{q}_{12}{}^T \tag{27}$$

By substituting Eq. (24) into Eq. (19), the sub-system is derived in the following form.

$$\dot{\boldsymbol{\xi}}_1 = \widehat{\boldsymbol{A}}_{11} \boldsymbol{\xi}_1 + \boldsymbol{A}_{12} v \tag{28}$$

$$\widehat{\boldsymbol{A}}_{11} = \boldsymbol{A}_{11} - \boldsymbol{A}_{12} q_{22}{}^{-1} \boldsymbol{q}_{12}{}^T \tag{29}$$

For the system (28), the solution of the optimal control problem gives v to minimize J_s as:

$$v = -q_{22}{}^{-1} \boldsymbol{A}_{12}{}^T \boldsymbol{P}_s \boldsymbol{\xi}_1 \tag{30}$$

In Eq. (30), $\boldsymbol{P}_s$, which indicates a unique positive-definite symmetric solution, can be obtained by solving the algebraic Riccati equation below.

$$\boldsymbol{P}_s \widehat{\boldsymbol{A}}_{11} + \widehat{\boldsymbol{A}}_{11}{}^T \boldsymbol{P}_s - \boldsymbol{P}_s \boldsymbol{A}_{12} q_{22}{}^{-1} \boldsymbol{A}_{12}{}^T \boldsymbol{P}_s + \widehat{\boldsymbol{q}}_{11} = 0 \tag{31}$$

Based on Eqs. (24) and (30), the switching function σ can be specified as:

$$\sigma = \boldsymbol{S} \boldsymbol{x}_{MF} = [\boldsymbol{A}_{12}{}^T \boldsymbol{P}_s + \boldsymbol{q}_{12}{}^T \quad q_{22}] \boldsymbol{T}_{tr} \boldsymbol{x}_{MF} \tag{32}$$

For Eq. (32), the sliding surface is defined as $\sigma = 0$ in the state-space.

3.2. Nonlinear switching control input and convergence analysis

To guarantee the reaching condition of the state trajectory towards the sliding surface and convergence to the origin, one candidate for such control laws is defined as [56]

$$\begin{aligned} u &= u_{eq} + u_{nl} \\ &= -(\boldsymbol{S}\boldsymbol{B}_{MF2})^{-1} \boldsymbol{S} \boldsymbol{A}_{MF} \boldsymbol{x}_{MF} - k|\sigma|^{-\alpha} \mathrm{sgn}(\sigma) \end{aligned} \tag{33}$$

where k is a switching gain and α is a positive variable in $0 < \alpha < 1$ [57].

For the control input (33), the reaching condition (i.e., the existence condition of the sliding mode) for $\sigma \to 0$ should be satisfied by the appropriate switching control input. To analyze this condition, the Lyapunov function technique is used [40][31]. The Lyapunov function of the switching function σ can be selected as:

$$V = \frac{1}{2}\sigma^2 > 0 \tag{34}$$

Considering the time derivative of V, the condition for $\sigma \to 0$ can be described as:

$$\dot{V} = \sigma^T \dot{\sigma} < 0 \ \text{ for } \forall \sigma \neq 0 \tag{35}$$

Note that σ is a scalar. The time derivative $\dot{V}$ is rearranged by substituting Eq. (33) into Eq. (35) as:

$$\begin{aligned}
\dot{V} &= \sigma^T \dot{\sigma} = \sigma^T \boldsymbol{S} \dot{\boldsymbol{x}}_{MF} \\
&= \sigma^T \boldsymbol{S} \{\boldsymbol{A}_{MF} \boldsymbol{x}_{MF} + \boldsymbol{B}_{MF1} w + \boldsymbol{B}_{MF2} u\} \\
&= \sigma^T \{\boldsymbol{S}\boldsymbol{A}_{MF} \boldsymbol{x}_{MF} + \boldsymbol{S}\boldsymbol{B}_{MF1} w - \boldsymbol{S}\boldsymbol{B}_{MF2} (\boldsymbol{S}\boldsymbol{B}_{MF2})^{-1} \boldsymbol{S}\boldsymbol{A}_{MF} \boldsymbol{x}_{MF} - k \boldsymbol{S}\boldsymbol{B}_{MF2} |\sigma|^{-\alpha} \mathrm{sgn}(\sigma)\} \\
&= \sigma^T \boldsymbol{S} \left\{ \boldsymbol{B}_{MF1} w - k \boldsymbol{B}_{MF2} |\sigma|^{-\alpha} \frac{\sigma}{|\sigma|} \right\}
\end{aligned} \tag{36}$$

For Eq. (36), condition (37) is equivalent to satisfying (35).

$$\begin{gathered}
\sigma^T \boldsymbol{S} \left\{ \boldsymbol{B}_{MF1} w - k \boldsymbol{B}_{MF2} |\sigma|^{-\alpha} \frac{\sigma}{|\sigma|} \right\} < 0 \\
\mathrm{sgn}(\sigma) \boldsymbol{S}\boldsymbol{B}_{MF1} w < k'
\end{gathered} \tag{37}$$

Here,

$$k' = k |\sigma|^{-\alpha} \boldsymbol{S}\boldsymbol{B}_{MF2} \tag{38}$$

In VCO-MFC, the unique point is that $T_{xvx1} \approx 1$ (i.e., $x_v \approx x_1$) is established by satisfying Eq. (4). Therefore, according to Eq. (5) with $c_v = 0$, w can be rewritten as:

$$w = k_v x_1 \approx k_v x_v = k_v [1 \quad 0 \quad 0 \quad 0] \begin{bmatrix} x_v \\ x_a \\ \dot{x}_v \\ \dot{x}_a \end{bmatrix} = k_v [1 \quad 0 \quad 0 \quad 0] \boldsymbol{x}_{MF} \tag{39}$$

The condition (37) is more specifically evaluated with Eq. (39) as follows.

$$\begin{aligned}
&\mathrm{sgn}(\sigma) \boldsymbol{S}\boldsymbol{B}_{MF1} w \approx \mathrm{sgn}(\sigma) \boldsymbol{S}\boldsymbol{B}_{MF1} k_v [1 \quad 0 \quad 0 \quad 0] \boldsymbol{x}_{MF} \\
&= \mathrm{sgn}(\sigma) \boldsymbol{S} k_v \begin{bmatrix} 0 \\ 0 \\ \dfrac{1}{m_v} \\ 0 \end{bmatrix} [1 \quad 0 \quad 0 \quad 0] \boldsymbol{x}_{MF} = \mathrm{sgn}(\sigma) \boldsymbol{S} \begin{bmatrix} 0 & 0 & 0 & 0 \\ 0 & 0 & 0 & 0 \\ \dfrac{k_v}{m_v} & 0 & 0 & 0 \\ 0 & 0 & 0 & 0 \end{bmatrix} \boldsymbol{x}_{MF} \\
&\leq \|\boldsymbol{S}\| \frac{k_v}{m_v} \|\boldsymbol{x}_{MF}\| \leq \|\boldsymbol{S}\| \frac{k_v}{m_v} \|\boldsymbol{x}_{MF}\|_{max}
\end{aligned} \tag{40}$$

Here, $\|\boldsymbol{x}_{MF}\|_{max}$ is the upper bound of norm of the state vector $\boldsymbol{x}_{MF}$. Combining Eqs. (37), (38) and (40), the following condition can be derived to guarantee the existence of the sliding mode.

$$\begin{gathered}
\|\boldsymbol{S}\| \frac{k_v}{m_v} \|\boldsymbol{x}_{MF}\|_{max} < k |\sigma|^{-\alpha} \boldsymbol{S}\boldsymbol{B}_{MF2} = (k'' (\boldsymbol{S}\boldsymbol{B}_{MF2})^{-1} |\sigma|^{\alpha}) |\sigma|^{-\alpha} \boldsymbol{S}\boldsymbol{B}_{MF2} = k'' \\
\|\boldsymbol{S}\| \frac{k_v}{m_v} \|\boldsymbol{x}_{MF}\|_{max} < k''
\end{gathered} \tag{41}$$

$$k = k'' (\boldsymbol{S}\boldsymbol{B}_{MF2})^{-1} |\sigma|^{\alpha} \tag{42}$$

The switching gain k'' of the control input must satisfy Eq. (41) for $\sigma \to 0$. Consequently, the control input is combination of the equivalent control input $u_{eq} = -(\boldsymbol{S}\boldsymbol{B}_{MF2})^{-1} \boldsymbol{S}\boldsymbol{A}_{MF} \boldsymbol{x}_{MF}$ and the nonlinear switching control input $u_{nl} = -k'' (\boldsymbol{S}\boldsymbol{B}_{MF2})^{-1} \mathrm{sgn}(\sigma)$ as:

$$u = -(\boldsymbol{S}\boldsymbol{B}_{MF2})^{-1} \boldsymbol{S}\boldsymbol{A}_{MF} \boldsymbol{x}_{MF} - k'' (\boldsymbol{S}\boldsymbol{B}_{MF2})^{-1} \mathrm{sgn}(\sigma) \tag{43}$$

$$\|\boldsymbol{S}\|\frac{k_v}{m_v}\|\boldsymbol{x}_{MF}\|_{max} < k'' \tag{44}$$

In this study, k'' is set as 1.0×10^1 to satisfy the inequality (44).

Note that $\|\boldsymbol{x}_{MF}\|_{max}$ does not need to be known in real implementations. This is because fluctuations of $\|\boldsymbol{x}_{MF}\|$ can be estimated by a Kalman filter, and the estimated value $\|\hat{\boldsymbol{x}}_{MF}\|$ is online evaluated in the condition (44) instead of $\|\boldsymbol{x}_{MF}\|_{max}$. The Kalman filer is designed for the system (6) composed of the VCO and actuator, meaning the model-free design [29]. Therefore, the reaching condition (35) (i.e., $\sigma \to 0$) can always be satisfied by modifying u_{nl} as follows:

$$u_{nl} = \begin{cases} -k''(\boldsymbol{SB}_{MF2})^{-1}\|\hat{\boldsymbol{x}}_{MF}\|\mathrm{sgn}(\sigma), & \|\boldsymbol{S}\|\frac{k_v}{m_v}\|\hat{\boldsymbol{x}}_{MF}\| \geq k'' \\ -k''(\boldsymbol{SB}_{MF2})^{-1}\mathrm{sgn}(\sigma), & \|\boldsymbol{S}\|\frac{k_v}{m_v}\|\hat{\boldsymbol{x}}_{MF}\| < k'' \end{cases} \tag{45}$$

$$\|\boldsymbol{S}\|\frac{k_v}{m_v} < k'' \tag{46}$$

4. VCO-based model-free fuzzy sliding mode control (VCO-MFFSMC)

4.1. Introduction of fuzzy rules

Employing the control law (43) causes severe chattering [31], [58], which may damage the hardware of the control system. This phenomenon originates from the sign function in u_{nl}.

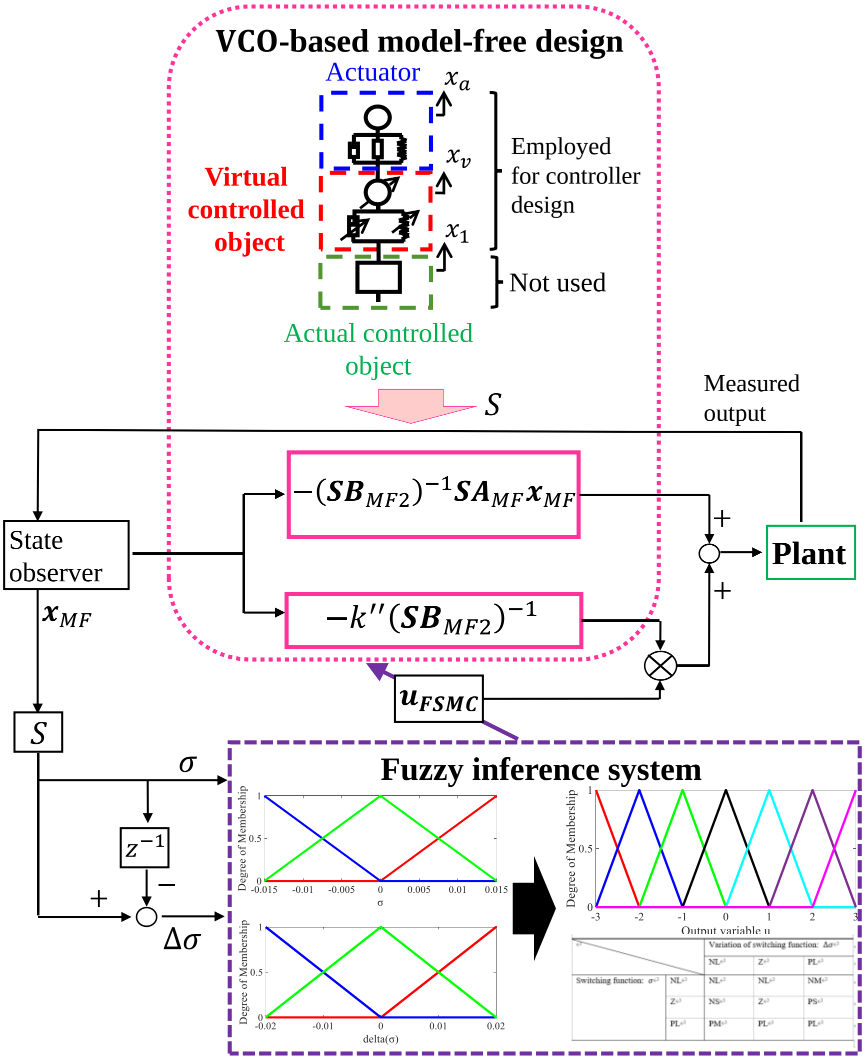

Fig. 4: Outline of the proposed control system.

In this section, an adaptive compensation law based on fuzzy inference is introduced to reduce the chattering phenomenon. This introduction results in the proposed VCO-MFFSMC, which is outlined in Fig. 4. The fuzzy inference aims to guide and constrain the state trajectory to the sliding surface ($\sigma = 0$) while avoiding drastic switching of the control input, which leads to chattering. Therefore, unlike standard SMCs, the rate of change of the switching function $\Delta\sigma$ also needs to be considered for computing the control input.

To always ensure $\sigma \to 0$, the basic spirit of the fuzzy rules is as follows [59]. If σ is rapidly drifting away from $\sigma = 0$ and $\Delta\sigma$ is also accelerating this departure, a large control input is needed to return the state trajectory to the sliding surface. On the other hand, if the positive and negative signs of σ and $\Delta\sigma$ differ (i.e., σ is naturally approaching $\sigma = 0$), the control effort should be decreased. Finally, a small control input should be applied to the system when the state trajectory is near $\sigma = 0$.

Let the switching function σ and the rate of change $\Delta\sigma$ be the input linguistic variables of the fuzzy inference, and the control input effort u_f be the output linguistic variable. The nine fuzzy rules, constructed according to the previous literature [59], are as follows:

(Rule 1).

IF (σ is **Negative Large (NL)**) and ($\Delta\sigma$ is **Negative Large (NL)**) THEN (u_f is **Negative Large (NL)**) (47)

(Rule 2).

IF (σ is **Negative Large (NL)**) and ($\Delta\sigma$ is **Zero (Z)**) THEN (u_f is **Negative Large (NL)**) (48)

(Rule 3).

IF (σ is **Negative Large (NL)**) and ($\Delta\sigma$ is **Positive Large (PL)**) THEN (u_f is **Negative Medium (NM)**) (49)

(Rule 4).

IF (σ is **Zero (Z)**) and ($\Delta\sigma$ is **Negative Large (NL)**) THEN (u_f is **Negative Small (NS)**) (50)

(Rule 5).

IF (σ is **Zero (Z)**) and ($\Delta\sigma$ is **Zero (Z)**) THEN (u_f is **Zero (Z)**) (51)

(Rule 6).

IF (σ is **Zero (Z)**) and ($\Delta\sigma$ is **Positive Large (PL)**) THEN (u_f is **Positive Small (PS)**) (52)

(Rule 7).

IF (σ is **Positive Large (PL)**) and ($\Delta\sigma$ is **Negative Large (NL)**) THEN (u_f is **Positive Medium (PM)**) (53)

(Rule 8).

IF (σ is **Positive Large (PL)**) and ($\Delta\sigma$ is **Zero (Z)**) THEN (u_f is **Positive Large (PL)**) (54)

(Rule 9).

IF (σ is **Positive Large (PL)**) and ($\Delta\sigma$ is **Positive Large (PL)**) THEN (u_f is **Positive Large (PL)**) (55)

The above fuzzy rules are summarized in a rule table, as shown in Table 2 [59].

Table 2. Fuzzy rule table of Rules 1-9 in (47)-(55)

		Variation of switching function: $\Delta\sigma$		
		NL	Z	PL
Switching function: σ	NL	NL	NL	NM
	Z	NS	Z	PS
	PL	PM	PL	PL

4.2. Fuzzy inference by Mamdani method

In this study, we applied the Mamdani inference method [60]. The triangular membership functions of the fuzzy sets with respect to σ, $\Delta\sigma$ and u_f are indicated in Fig. 5(a), (b), and (c), respectively. The output of each rule is computed by reflecting the degree of match of each fuzzy rule $0 \leq w_i \leq 1$ $(i = 1-9)$ on the consequent proposition as:

$$h_i^*(u_f) = w_i \cdot h_i^u(u_f) \tag{56}$$

where $h_i^u(u_f)$ $(i = 1-9)$ is the membership function of the fuzzy sets of u_f in the consequent part, corresponding to one of {**NL**, **NM**, **NS**, **Z**, **PS**, **PM**, **PL**}. The resultant output considering all of Rules 1-9 is then obtained by integrating each result $h_i^*(u_f)$ as:

$$h_{FSMC}(u_f) = \max_{i=1-9} h_i^*(u_f). \tag{57}$$

In the defuzzification process to convert the inference result in Eq. (57) into a crisp value, a center-of-gravity computing method for $h_{FSMC}(u_f)$ gives the fuzzy control input u_{FSMC} as:

$$u_{FSMC} = \frac{\int u_f \cdot h_{FSMC}(u_f)\, du_f}{\int h_{FSMC}(u_f)\, du_f}. \tag{58}$$

To construct VCO-MFFSMC, $\mathrm{sgn}(\sigma)$ in Eq. (43) is replaced with u_{FSMC} as:

$$u = -(\boldsymbol{SB}_{MF2})^{-1}\boldsymbol{SA}_{MF}\boldsymbol{x}_{MF} - k''(\boldsymbol{SB}_{MF2})^{-1}u_{FSMC} \tag{59}$$

By replacing $\mathrm{sgn}(\sigma)$, which leads to intensive discontinuous changes of the control input, with u_{FSMC}, severe chattering can be prevented. Unlike standard SMC, the consideration of $\Delta\sigma$ for managing the control input amount also contributes to the mitigation of chattering. The parameters used for VCO-MFFSMC are indicated in Table 3. These values are determined based on manual tuning. The appropriate value of these parameters will vary depending on the specific applications. The employed membership functions are indicated in Fig. 5. In this study, "Control System Toolbox" in MATLAB was employed for controller design.

Table 3. Parameters for the control system design

Properties	Value
$\boldsymbol{W}$	$diag\{10^{-20} \quad 10^{-20} \quad 10^{-20} \quad 10^{-30}\}$
k''	1.0×10^1

Figure 5 shows the membership functions used in the proposed fuzzy inference compensation for chattering reduction. The triangular membership functions of the fuzzy sets with respect to σ, $\Delta\sigma$ and u_f are indicated in Fig. 5(a), (b), and (c), respectively. These functions are regarded as designer-defined tuning variables. For σ and $\Delta\sigma$ in the input part of the above fuzzy rules, the linguistic fuzzy sets: **Positive Large (PL)**, **Zero** and **Negative Large (NL)** are expressed by the red, black, and blue lines, respectively. For u_f in the output part of the fuzzy rules, the fuzzy sets: **Positive Large (PL)**, **Positive Medium (PM)**, **Positive Small (PS)**, **Zero**, **Negative Small (NS)**, **Negative Medium (NM)** and **Negative Large (NL)** are described by the seven triangular membership functions, as shown in Fig. 5(c). When designing the fuzzy sliding mode controller, selections of the appropriate membership functions are crucial for improving control performance, which may require some trial-and-error adjustments according to design policies based on both qualitative and quantitative viewpoints.

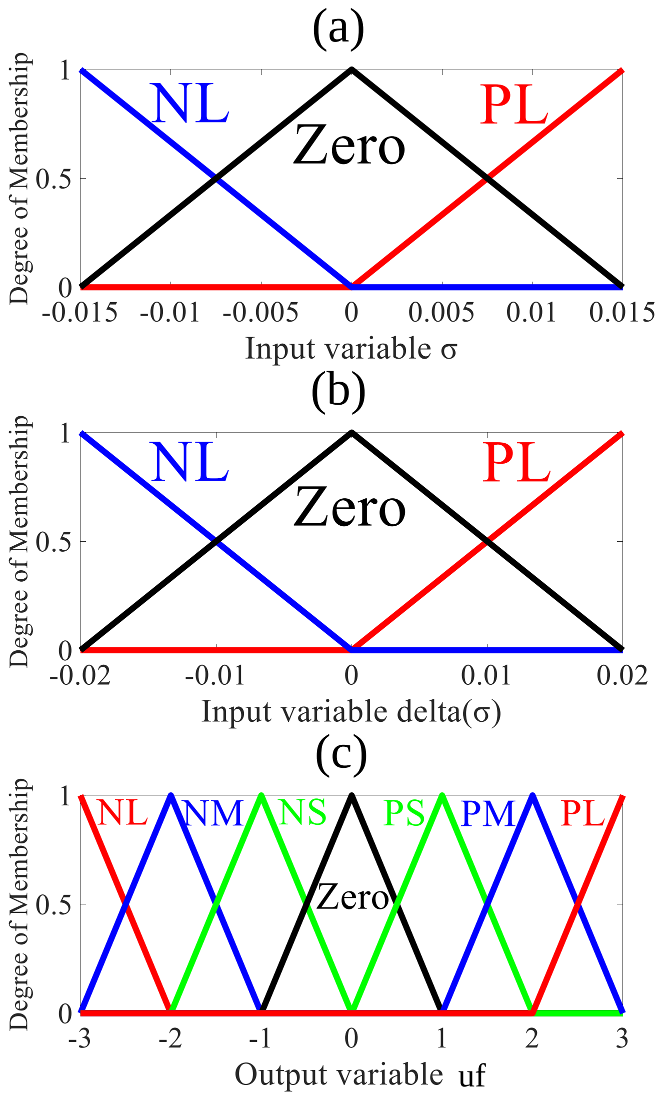

Fig. 5: Triangular membership functions of the fuzzy sets: (a) switching function, (b) variation of the switching function, and (c) control effort.

5. Vibration control simulations

We demonstrate the superiority of the proposed control scheme via vibration control simulations. Specifically, in Section 5.1, we examine the validity of the fuzzy logic-based chattering attenuation strategy using the finite element structures as the controlled object. In Section 5.2, we compare the VCO-MFFSMC with a conventional model-based vibration controller through vibration control simulations with the structures with time-varying properties, demonstrating the virtue of the VCO-based model-free control framework. For each control method, one same controller is consistently applied to all the controlled structures appearing in this paper.

5.1. Verification of the chattering reduction ability of the proposed approach

In this section, the VCO-MFFSMC is compared with the previous approach, which is the VCO-based model free SMC proposed in the earlier study [29]. The conventional controller lacks fuzzy inference and employs only a smoothing function for chattering reduction. The aim of this comparison is to demonstrate the chattering elimination effect of the proposed fuzzy logic-based strategy for VCO-based model-free SMC under the practical implementation situation.

Figure 6 shows an overview of the controlled structures in this section. Controlled object 1 shown in Fig 6(a) is composed of the cantilever plate (dimension: 248×190×10 mm) and two blocks (dimension: 100×26×30mm) attached on as weights on the backside of it. Controlled object 2 described in Fig. 6(b) is the both-ends supported plate (dimension: 342×100×10 mm) where one block weight (dimension: 26×100×30mm) is attached to the backside of it. The locations where the blocks are attached as weights are indicated by broken lines. The values of the Young modulus, Poisson ratio, and density for the cantilever plate and the both-ends-supported plate are about 75 GPa, 0.31, and 2700 kg/m^3, respectively. These for the weights are 206 GPa, 0.29, and 7800 kg/m^3, respectively. Note that both Controlled objects 1 and 2 have many resonant modes. The mode shapes are not trivial due to the block weights. Therefore, Controlled objects 1 and 2 reflect the representative intractability that are often observed in real applications.

The disturbance to shake the structures and the control input to actively suppress the vibrations are applied at locations A and B, respectively, at location C, the measured acceleration response is obtained. When the disturbance applied at location A excites the structure, the aim is to suppress the vibration at location C by the control input applied from location B. Considering the existence of amplifiers and signal communication used in real applications, a delay element of approximately 3.5×10^{-4} s is introduced in applying the control input. Such ignored dynamics in actuators, sensors, and signal processors are a typical cause of chattering in practice [61]. Because the collocation of actuator mounting and output measurement has to be approximately satisfied for model-free control [24], location C corresponds to location B on the back side of the plate. The disturbance is a linear sweep sinusoidal signal of 1–3000 Hz.

For performing simulations, dynamical models of the structures combined with the actuator are derived based on finite element analysis using ANSYS [62], [63]. A 20-node hexahedron is employed for finite element modeling of Controlled objects 1 and 2. The total numbers of nodes of the finite element model are 4748 and 21950 for Controlled objects 1 and 2, respectively. This study performed theoretical modal analysis by considering an undamped vibration system for an equation of motion of the controlled structure. By solving the eigenvalue problem for this model, the physical model was transformed into the modal model via modal coordinate transformation [62]. In the modal coordinate system, a same modal damping ratio of 0.5% was uniformly given to all the employed modes.

Figures 7 and 8 show the simulation results for Controlled objects 1 and 2, respectively. The lower graph depicts the time response of the control signal, while the upper graph depicts the acceleration response. The blue line represents the open-loop response without any controls. The red and black lines indicate the control results with VCO-MFFSMC and the previous approach, respectively. For the major resonance peaks appearing between 0 s and 10 s, both the VCO-MFFSMC and the previous approach sufficiently suppress the vibration amplitude and exhibit good damping capability compared to the open-loop response. Nevertheless, as shown by the black line, the intensive chattering phenomenon is consistently observed in the previous approach. The remaining chattering implies that a simple countermeasure merely using smoothing functions (e.g., hyperbolic tangent [29]) is insufficient depending on the controlled objects. In contrast, the proposed approach (VCO-MFFSMC), shown by the red line, considerably reduces the chattering. This benefit is due to the introduction of fuzzy-inference-based compensation.

Tables 4 and 5 show the approximate reductions for the major peaks when the frequency responses are evaluated for Controlled objects 1 and 2, respectively. Compared to VCO-MFFSMC, the reduction amounts of the previous approach are degraded at the 306 Hz peak of Controlled object 1 and the 234 Hz peak of Controlled object 2. The cause of these degradations is considered to be the effects of the induced chattering.

In Tables 6 and 7, VCO-MFFSMC achieves the minimum value of the 2-norm of the acceleration response, which quantitatively indicates improved vibration control. In contrast, for Controlled object 1, the larger 2-norm of the previous approach compared to the open-loop response indicates performance aggravation due to the persistent chattering effect. This is also evident from the significant difference in the 2-norm of the control input between VCO-MFFSMC and the previous approach.

Consequently, the comparative result shown in Figs 7 and 8 and Tables 4–7 clearly demonstrates the advantage of fuzzy inference for chattering reduction.

Table 4. Vibration reduction amount for major resonance peaks for Controlled object 1.

Controller	Reduction amount	
	148 Hz peak	306 Hz peak
VCO-MFFSMC	21.9200 dB	8.2900 dB
Previous approach	22.3200 dB	3.6100 dB

Table 5. Vibration reduction amount for major resonance peaks for Controlled object 2.

Controller	Reduction amount
	234 Hz peak
VCO-MFFSMC	18.5300 dB
Previous approach	12.7900 dB

Table 6. 2-norm of the vibration response and control input for Controlled object 1.

Controller	2-norm	
	Acceleration response	Control input
VCO-MFFSMC	1.5328×10^3	140.0167
Previous approach	3.6867×10^3	572.6513
Open-loop	2.1270×10^3	–

Table 7. 2-norm of the vibration response and control input for Controlled object 2.

Controller	2-norm	
	Acceleration response	Control input
VCO-MFFSMC	2.9089×10^3	70.0133
Previous approach	3.1714×10^3	311.0785
Open-loop	3.2474×10^3	–

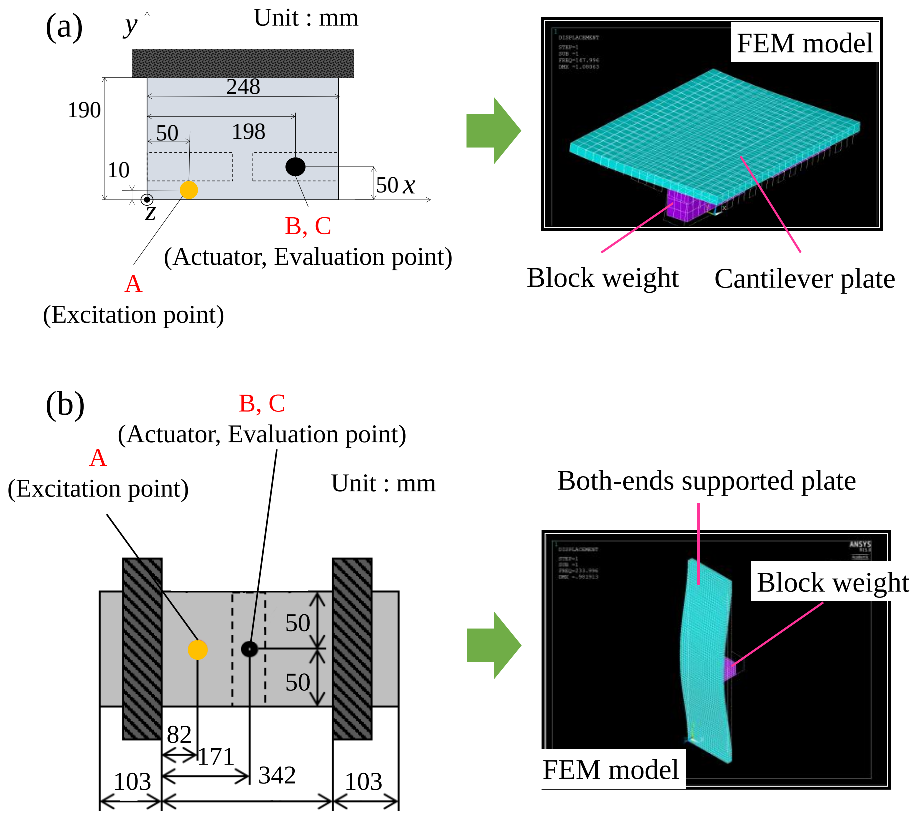

Fig. 6: Configurations of controlled objects: (a) cantilever plate (Controlled object 1) and (b) both-ends-supported plate (Controlled object 2). The locations where the blocks are attached as weights are indicated by broken lines.

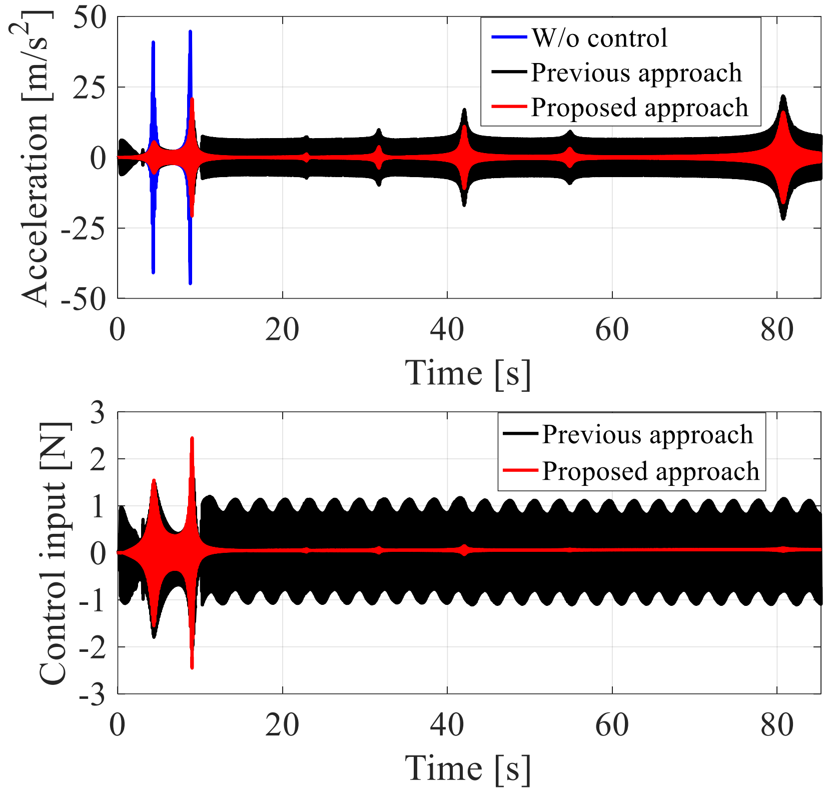

Fig. 7: Time responses of the acceleration and control input in simulation for the cantilever plate (Controlled object 1).

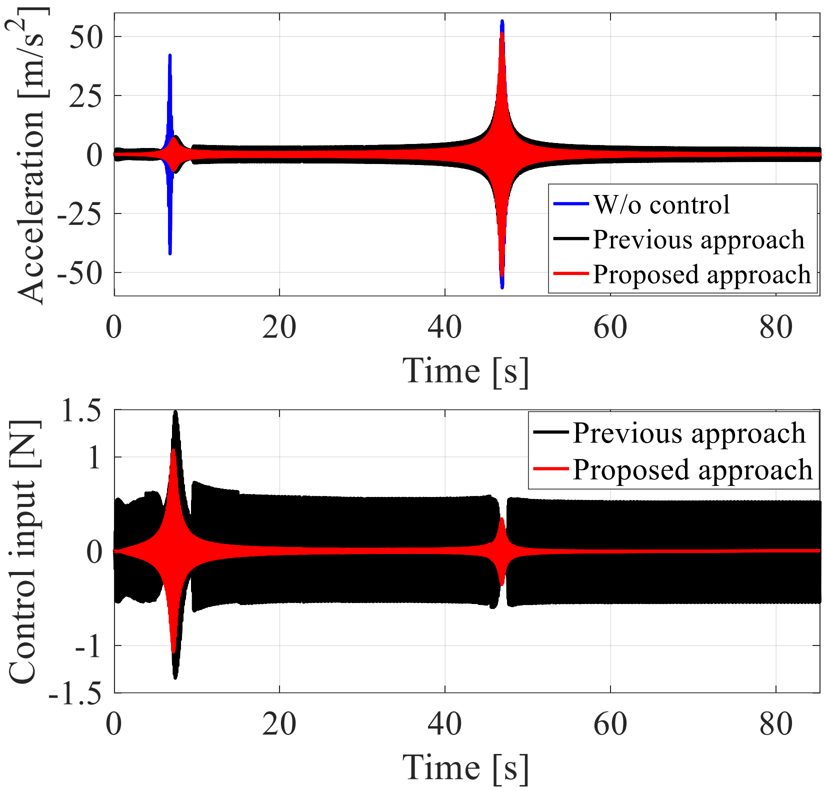

Fig. 8: Time responses of the acceleration and control input in simulation for the both-ends-supported plate (Controlled object 2).

5.2. Comparative study with model-based controller

In this section, the VCO-MFFSMC and the conventional VCO-based SMC are compared with the traditional model-based controller in order to demonstrate the advantage of the VCO-based model-free framework. The controlled object is the two-degree-of-freedom (2DOF) vibration systems with time-varying specifications [26]: Controlled object 3 involves online perturbed mass variations, and Controlled object 4 involves online perturbed spring constants. The model structure and specifications are shown in Fig. 9 and Table 8, respectively. The model-based controller is designed by applying the linear H_2 control theory [64], [65] to the system composed of the actuator and the 2DOF structure shown in Fig. 9, where the time-varying property is ignored. The parameter values of the model for designing the H_2 controller are the medium values shown in Table 8. The details of the comparison procedure are as follows:

Step 1) The control performances of the VCO-MFFSMC and the model-based H_2 controller are unified through the vibration control simulation using the 2DOF structure used for designing the H_2 controller. Specifically, the VCO-MFFSMC and the model-based H_2 controller are applied to a time-invariant 2DOF system with fixed specifications, which are the medium values shown in Table 8. In this simulation, the model-based H_2 controller is tuned so that its vibration performance matches that of the VCO-MFFSMC, which has been applied to Controlled objects

1 and 2 in the previous section.

Step 2) The VCO-MFFSMC, the previous model-free SMC, and the model-based H_2 controller are applied to the vibration control simulation for the time-varying 2DOF systems, i.e., Controlled object 3 and Controlled object 4. Each controller is the same as that used in Step 1.

As a performance index for the time-varying system, we evaluate a loss function with respect to the controlled output in Step 2. As shown in Eq. (60), the loss function $L(k)$ is defined as the mean-square of the measured output in the k-th evaluation interval, presenting a quantitative performance index suitable for time-varying systems [26][66]:

$$L(k) = \frac{1}{f_s} \sum_{j=(k-1)m+1}^{km} y(j)^2 \tag{60}$$

where m indicates the number of evaluation points in each evaluation interval, f_s denotes the sampling frequency, and y is the measured acceleration response of the real controlled object. Here, j indicates the number of sampling points. Random noise was used as the excitation disturbance in Step 2.

Regarding Step 1, Fig. 10 shows the frequency response of the fixed 2DOF system (i.e., time-invariant system) from the disturbance, which is a 1-1000 Hz linear sweep sinusoidal signal, to the measured acceleration. We can see that the performance of VCO-MFFSMC and that of the model-based controller are almost the same. That is, the tuning of the model-based controller is properly achieved.

Figures 11–14 show the simulation results obtained at Step 2. Figures 11 and 12 show the time history of the loss function in Eq. (60) and the control result (upper graph: acceleration response and lower graph: control input), respectively, for Controlled object 3. Figures 13 and 14 show those for Controlled object 4. Here, random noise was used as the disturbance. In Figs. 11–14, the blue, black, green, and red lines indicate the response without control, the closed-loop response with the model-based H_2 controller, the closed-loop response with the VCO-based SMC, and the closed-loop response with the VCO-MFFSMC, respectively. Figures 11(b) and 13(b) describe the time history of the parameter values of Controlled objects 3 and 4, respectively.

According to Figs. 11–14, the VCO-based controllers successfully reduce the vibration occurring at Controlled objects 3 and 4, whereas the severe performance degradations are observed for the model-based H_2 controller. This result implies that the model-based approach requires the explicit consideration of the time-varying property of the actual controlled structure. Nevertheless, explicit consideration of the time-varying property significantly increases the design complexity and hence degrades the practical usability; this approach cannot handle the unknown time-varying characteristics. On the other hand, the VCO-based model-free controller (the VCO-MFFSMC) successfully reduces the vibration occurring at the time-varying 2DOF structures. Here, after the introduction of the VCO, the controller design procedure of VCO-MFC is exactly the same as the conventional model-based approach for the linear time-invariant system. Hence, the proposed VCO-based control framework significantly reduces the controller design procedure for challenging vibration control problems, which is the representative advantage over the conventional model-based controller design. Note that addressing known/unknown time-varying characteristics is a representative challenge for vibration controller design in practical mechanical systems.

Remark: The success of the VCO-based approach in this example is regarded as its model-free nature. That is, the VCO-based model-free controller is designed without using detailed mathematical models of an actual controlled structure, giving the insensitiveness of the resulting controller to the characteristic changes in actual controlled structure. The VCO-based controller works well as long as $x_v \approx x_1$ holds by Eq. (4). In fact, the same controller, including the values of its tuning parameters, consistently exhibits good vibration attenuation performance to Controlled objects 1–4 in this study. These results show the robustness of the VCO-based model-free controller to the characteristic changes in actual controlled object, which is an important virtue of the VCO-MFFSMC proposed in this study. In other words, the strong robustness of the VCO-MFFSMC comes from the VCO-based model-free design. Therefore, the proposed approach is superior to the traditional model-based controller in practical applications, since the real-world systems always have various uncertainties and characteristic changes.

Table 8. Model parameters of Controlled objects 3 and 4.

	Controlled object 3	Controlled object 4
m_1 [kg]	2.5 ± 2.0 (sinusoidally varying with a period of 25.6 s)	2.5
m_2 [kg]	2.5 ± 2.0 (sinusoidally varying with a period of 12.8 s)	2.5
k_1 [N/m]	1.0×10^6	$10^6 \pm 7.0 \times 10^5$ (sinusoidally varying with a period of 25.6 s)
k_2 [N/m]	1.0×10^6	$10^6 \pm 7.0 \times 10^5$ (sinusoidally varying with a period of 12.8 s)
c_1 [Ns/m]	15.8114	15.8114
c_2 [Ns/m]	15.8114	15.8114

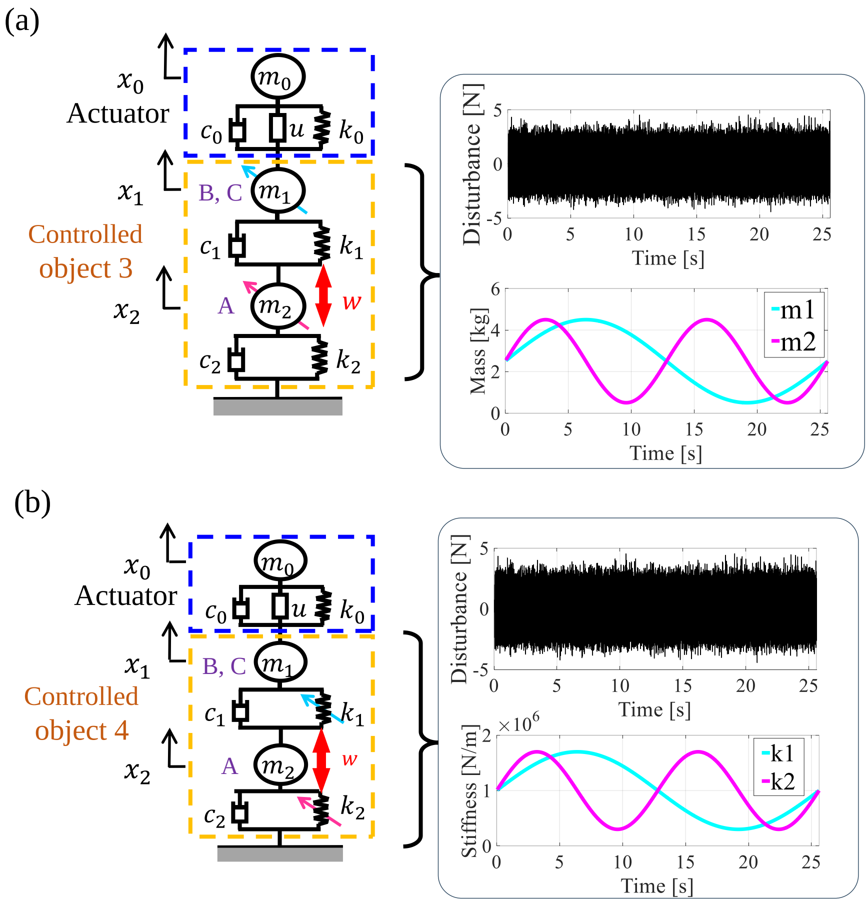

Fig. 9: Configurations of controlled objects: (a) Controlled object 3 and (b) Controlled object 4.

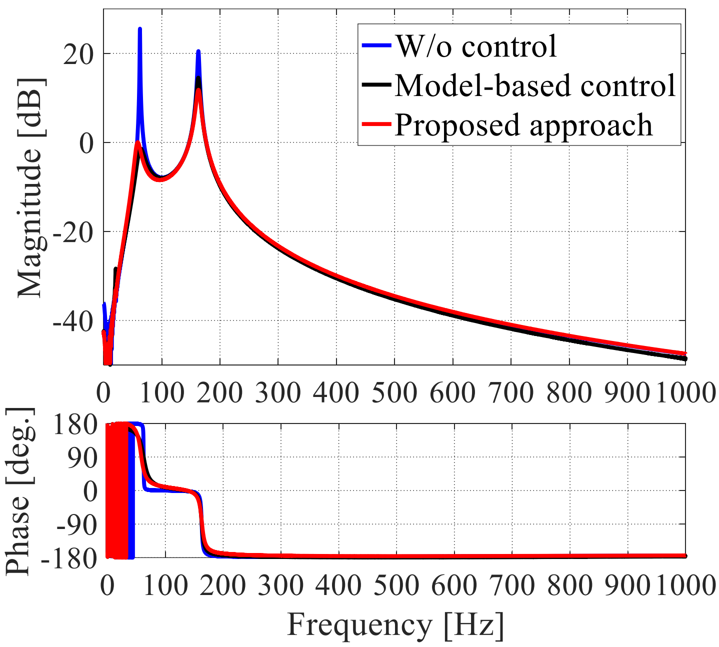

Fig. 10: Frequency response of the fixed 2DOF system (i.e., time-invariant system).

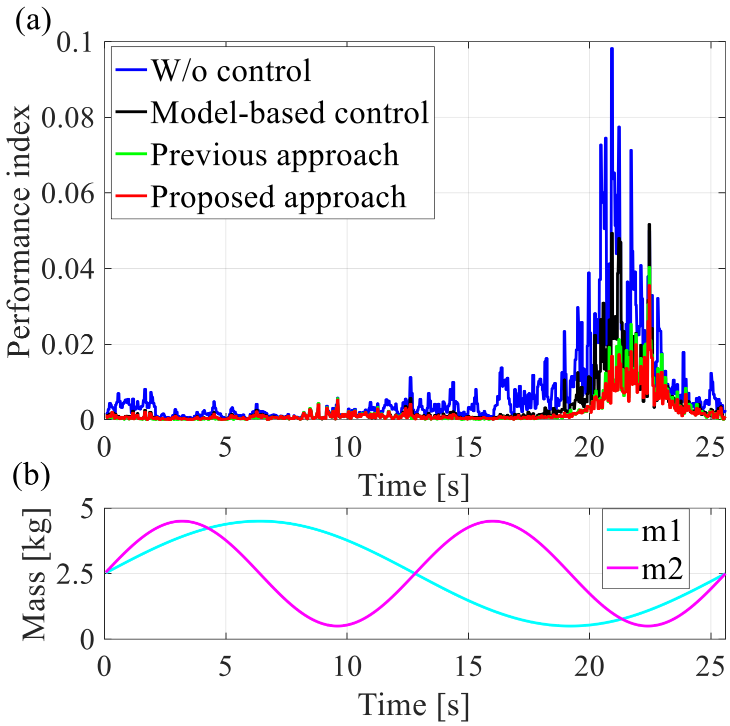

Fig. 11: Time histories of the performance index values for Controlled object 3.

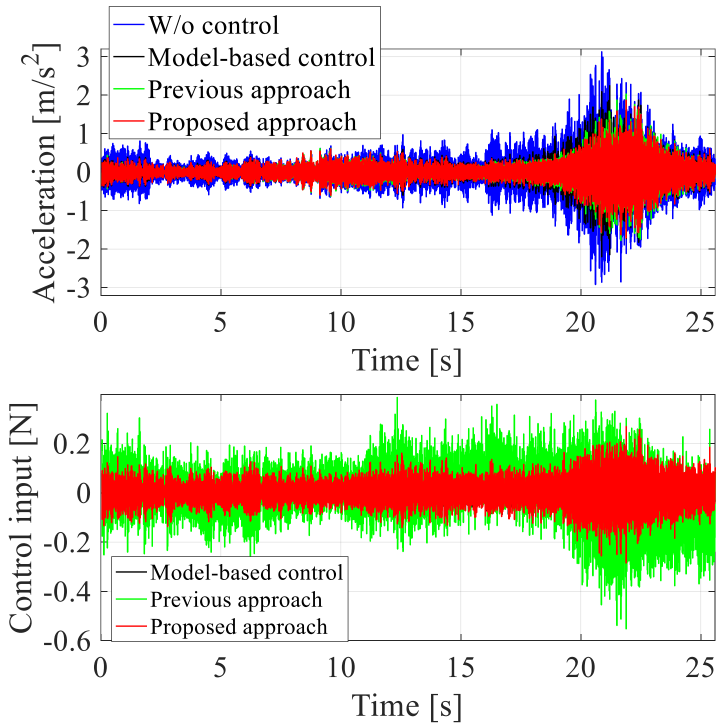

Fig. 12: Time responses of the acceleration and control input for Controlled object 3.

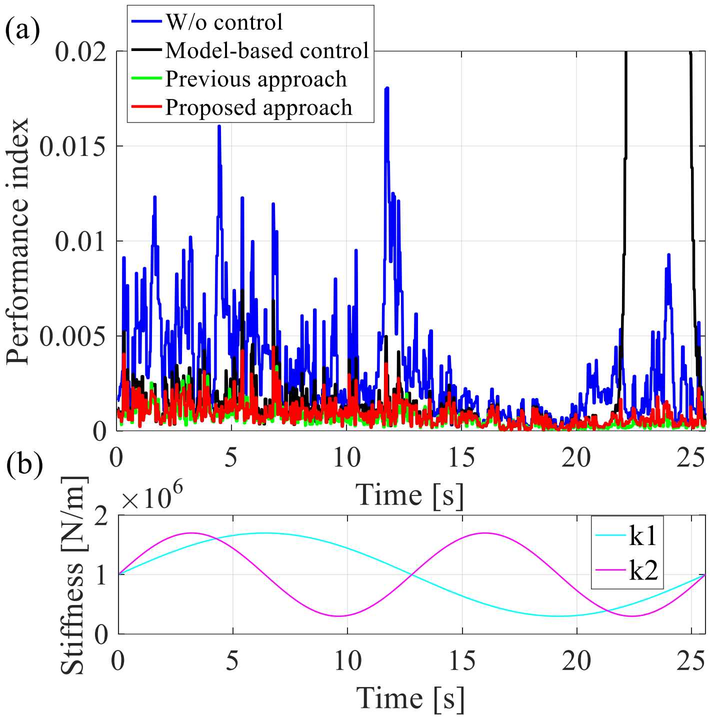

Fig. 13: Time histories of the performance index values for Controlled object 4.

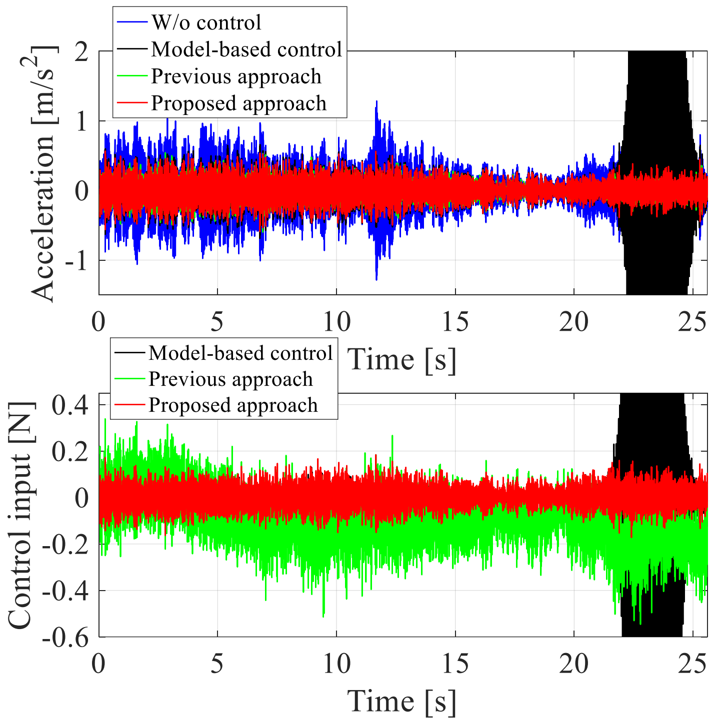

Fig. 14: Time responses of the acceleration and control input for Controlled object 4.

6. Conclusion

Based on the concept of VCO, this study proposed a novel fuzzy sliding mode vibration controller that is free from any mathematical modeling of real controller objects. The key idea is the combination of the

VCO-based MFC, sliding mode control, and fuzzy adaptive compensation for chattering elimination. The development of the model-free sliding mode vibration controller was easily achieved by simply setting the SDOF VCO, and the convergence was analyzed using a Lyapunov function technique. To compensate for the chattering phenomenon, fuzzy inference was further integrated into the model-free SMC. The fuzzy rules were constructed to hindering the occurrence of severe chattering while ensuring that the system state is rapidly guided toward the sliding surface. Finally, the proposed approach was verified through the several control simulations with various mechanical structures, including a time-varying system. The high damping performance of the proposed model-free fuzzy SMC, as well as its robustness to changes in the controlled objects, was confirmed via comparisons to existing approaches.
The future direction of this work will focus on the introduction of optimization techniques for designing the membership functions and compensations for actuator uncertainty and observation noise.

Acknowledgements
We thank the Japan Society for the Promotion of Science for their support under Grants-in-Aid for Scientific Research Programs (Grant 23K13273).

Author Contributions
HY: conceptualization, methodology, software, formal analysis, investigation, resources, data curation, writing original draft. AY: methodology, software, investigation, writing original draft. IK: conceptualization, methodology, supervision, writing original draft.

Funding
A part of this research was funded by the Japan Society for the Promotion of Science under Grants-in-Aid for Scientific Research Programs (Grant 23K13273).

Declarations
Conflict of Interest
On behalf of all authors, the corresponding author states that there is no conflict of interest.

References

1. MengTong W, Pan S, ShuYong L, et al (2023) Design and Analysis of Electromagnetic Quasi-zero Stiffness Vibration Isolator. J Vib Eng Technol 11:153–164. https://doi.org/10.1007/s42417-

022-00569-x
2. Zlatkov D, Ristić D, Zorić A, et al (2022) Experimental and Numerical Study of Energy Dissipation Components of a New Metallic Damper Device. J Vib Eng Technol 10:1809–1829. https://doi.org/10.1007/s42417-022-00485-0
3. Dal Bo L, Gardonio P, Battistella N, Turco E (2023) Non-linear Isolator for Vibration and Force Transmission Control of Unbalanced Rotating Machines. J Vib Eng Technol 11:1741–1764. https://doi.org/10.1007/s42417-022-00668-9
4. Salem MAM, Kassem M, Amin MS, et al (2024) Energy-Based Optimal Placement of Piezoelectric Actuator on Smart Thin Plate. J Vib Eng Technol 12:1813–1830. https://doi.org/10.1007/s42417-023-00944-2
5. Ghachi RF, Mohamed AS, Renno J, Alnahhal W (2023) Application of Metastructures for Targeted Low-Frequency Vibration Suppression in Plates. J Vib Eng Technol 11:887–897. https://doi.org/10.1007/s42417-022-00614-9
6. Han B, Ji H, Wang C, et al (2024) Aperiodic Two-Dimensional Acoustic Black Holes for Broadband Vibration Attenuation in a Strip. J Vib Eng Technol. https://doi.org/10.1007/s42417-024-01360-w
7. Werner U (2021) 3D Model for Active Vibration Control of Rotating Machines Mounted on Active Machine Foot Mounts Using Vibration Mode Coupling by Asymmetry. J Vib Eng Technol 9:613–641. https://doi.org/10.1007/s42417-020-00252-z
8. Werner U (2024) Active Vibration Control of a Rotating Machine with Voltage-Driven Electrodynamic Actuators Between Machine Feet and Steel Frame Foundation Under Multiple Base Excitations. J Vib Eng Technol 12:3977–4004. https://doi.org/10.1007/s42417-023-01100-6
9. Yonezawa H, Kajiwara I, Nishidome C, et al (2021) Active vibration control of automobile drivetrain with backlash considering time-varying long control period. Proc Inst Mech Eng Part D J Automob Eng 235:773–783. https://doi.org/10.1177/0954407020949428
10. Zhang M, Jing X, Wang G (2021) Bioinspired Nonlinear Dynamics-Based Adaptive Neural Network Control for Vehicle Suspension Systems With Uncertain/Unknown Dynamics and Input Delay. IEEE Trans Ind Electron 68:12646–12656. https://doi.org/10.1109/TIE.2020.3040667
11. Qiu Z, Zhang W (2019) Trajectory planning and diagonal recurrent neural network vibration control of a flexible manipulator using structural light sensor. Mech Syst Signal Process 132:563–594. https://doi.org/10.1016/j.ymssp.2019.07.014
12. Miao X, Yang L, Ouyang H (2023) Artificial-neural-network-based optimal Smoother design for oscillation suppression control of underactuated overhead cranes with distributed mass beams. Mech Syst Signal Process 200:110497. https://doi.org/10.1016/j.ymssp.2023.110497
13. Ariza-Zambrano WC, Serpa AL (2021) Direct inverse control for active vibration suppression using artificial neural networks. J Vib Control 27:31–42. https://doi.org/10.1177/1077546320924253

14. Song H, Shan X, Zhang L, et al (2022) Research on identification and active vibration control of cantilever structure based on NARX neural network. Mech Syst Signal Process 171:108872. https://doi.org/10.1016/j.ymssp.2022.108872
15. Wang M, Fang X, Wang Y, et al (2023) A dual-loop active vibration control technology with an RBF-RLS adaptive algorithm. Mech Syst Signal Process 191:110079. https://doi.org/10.1016/j.ymssp.2022.110079
16. He W, Ouyang Y, Hong J (2017) Vibration Control of a Flexible Robotic Manipulator in the Presence of Input Deadzone. IEEE Trans Ind Informatics 13:48–59. https://doi.org/10.1109/TII.2016.2608739
17. Campi MC, Lecchini A, Savaresi SM (2002) Virtual reference feedback tuning: a direct method for the design of feedback controllers. Automatica 38:1337–1346. https://doi.org/10.1016/S0005-1098(02)00032-8
18. Campi MC, Savaresi SM (2006) Direct Nonlinear Control Design: The Virtual Reference Feedback Tuning (VRFT) Approach. IEEE Trans Automat Contr 51:14–27. https://doi.org/10.1109/TAC.2005.861689
19. Kaneko O (2013) Data-Driven Controller Tuning: FRIT approach. IFAC Proc Vol 46:326–336. https://doi.org/10.3182/20130703-3-FR-4038.00122
20. Yahagi S, Kajiwara I (2023) Noniterative Data-Driven Gain-Scheduled Controller Design Based on Fictitious Reference Signal. IEEE Access 11:55883–55894. https://doi.org/10.1109/ACCESS.2023.3278798
21. Yahagi S, Kajiwara I (2024) Data-driven design of model-free control for reference model tracking based on an ultra-local model: Application to vehicle yaw rate control. Proc Inst Mech Eng Part D J Automob Eng. https://doi.org/10.1177/09544070231215636
22. Yahagi S, Kajiwara I (2022) Direct Data-Driven Tuning of Look-Up Tables for Feedback Control Systems. IEEE Control Syst Lett 6:2966–2971. https://doi.org/10.1109/LCSYS.2022.3181343
23. Yahagi S, Kajiwara I (2022) Direct tuning method of gain-scheduled controllers with the sparse polynomials function. Asian J Control 24:2111–2126. https://doi.org/10.1002/asjc.2657
24. Yonezawa H, Kajiwara I, Yonezawa A (2020) Experimental verification of model-free active vibration control approach using virtually controlled object. JVC/Journal Vib Control 26:1656–1667. https://doi.org/10.1177/1077546320902348
25. Yonezawa A, Yonezawa H, Kajiwara I (2022) Parameter tuning technique for a model-free vibration control system based on a virtual controlled object. Mech Syst Signal Process 165:108313. https://doi.org/10.1016/j.ymssp.2021.108313
26. Yonezawa A, Yonezawa H, Kajiwara I (2022) Vibration control for various structures with time-varying properties via model-free adaptive controller based on virtual controlled object and SPSA. Mech Syst Signal Process 170:108801. https://doi.org/10.1016/j.ymssp.2022.108801
27. Yonezawa A, Yonezawa H, Kajiwara I (2023) Efficient parameter tuning to enhance practicability of a model-free vibration controller based on a virtual controlled object. Mech Syst

Signal Process 200:110526. https://doi.org/10.1016/j.ymssp.2023.110526
28. Yonezawa A, Yonezawa H, Kajiwara I (2023) Experimental study of model-free vibration control based on a virtual controlled object considering parameter uncertainty of actuator. Proc Inst Mech Eng Part C J Mech Eng Sci 237:2665–2674. https://doi.org/10.1177/09544062221140814
29. Yonezawa A, Kajiwara I, Yonezawa H (2021) Novel Sliding Mode Vibration Controller With Simple Model-Free Design and Compensation for Actuator's Uncertainty. IEEE Access 9:4351–4363. https://doi.org/10.1109/ACCESS.2020.3047810
30. Amirkhani S, Mobayen S, Iliaee N, et al (2019) Fast terminal sliding mode tracking control of nonlinear uncertain mass–spring system with experimental verifications. Int J Adv Robot Syst 16:172988141982817. https://doi.org/10.1177/1729881419828176
31. Shtessel Y, Edwards C, Fridman L, Levant A (2014) Sliding Mode Control and Observation. Birkhäuser, Basel, Switzerland
32. Fei J, Lu C (2018) Adaptive Sliding Mode Control of Dynamic Systems Using Double Loop Recurrent Neural Network Structure. IEEE Trans Neural Networks Learn Syst 29:1275–1286. https://doi.org/10.1109/TNNLS.2017.2672998
33. Tuan LA, Cuong HM, Trieu P Van, et al (2018) Adaptive neural network sliding mode control of shipboard container cranes considering actuator backlash. Mech Syst Signal Process 112:233–250. https://doi.org/10.1016/j.ymssp.2018.04.030
34. Chen S-A, Wang J-C, Yao M, Kim Y-B (2017) Improved optimal sliding mode control for a non-linear vehicle active suspension system. J Sound Vib 395:1–25. https://doi.org/10.1016/j.jsv.2017.02.017
35. Pusadkar US, Chaudhari SD, Shendge PD, Phadke SB (2019) Linear disturbance observer based sliding mode control for active suspension systems with non-ideal actuator. J Sound Vib 442:428–444. https://doi.org/10.1016/j.jsv.2018.11.003
36. Wang G, Chadli M, Basin M V. (2021) Practical Terminal Sliding Mode Control of Nonlinear Uncertain Active Suspension Systems With Adaptive Disturbance Observer. IEEE/ASME Trans Mechatronics 26:789–797. https://doi.org/10.1109/TMECH.2020.3000122
37. Wang J, Jin F, Zhou L, Li P (2019) Implementation of model-free motion control for active suspension systems. Mech Syst Signal Process 119:589–602. https://doi.org/10.1016/j.ymssp.2018.10.004
38. Liao K, He Z, Xu Y, et al (2017) A Sliding Mode Based Damping Control of DFIG for Interarea Power Oscillations. IEEE Trans Sustain Energy 8:258–267. https://doi.org/10.1109/TSTE.2016.2597306
39. Wan S, Li X, Su W, et al (2020) Active chatter suppression for milling process with sliding mode control and electromagnetic actuator. Mech Syst Signal Process 136:106528. https://doi.org/10.1016/j.ymssp.2019.106528
40. Khan AH, Li S (2020) Sliding Mode Control With PID Sliding Surface for Active Vibration Damping of Pneumatically Actuated Soft Robots. IEEE Access 8:88793–88800.

https://doi.org/10.1109/ACCESS.2020.2992997
41. Wang HP, Mustafa GIY, Tian Y (2018) Model-free fractional-order sliding mode control for an active vehicle suspension system. Adv Eng Softw 115:452–461. https://doi.org/10.1016/j.advengsoft.2017.11.001
42. Yiğit İ (2017) Model free sliding mode stabilizing control of a real rotary inverted pendulum. J Vib Control 23:1645–1662. https://doi.org/10.1177/1077546315598031
43. Ahmed S, Wang H, Tian Y (2018) Model-free control using time delay estimation and fractional-order nonsingular fast terminal sliding mode for uncertain lower-limb exoskeleton. J Vib Control 24:5273–5290. https://doi.org/10.1177/1077546317750978
44. Zhong G, Wang C, Dou W (2021) Fuzzy adaptive PID fast terminal sliding mode controller for a redundant manipulator. Mech Syst Signal Process 159:107577. https://doi.org/10.1016/j.ymssp.2020.107577
45. Yu Y, Yang Z, Han C, Liu H (2018) Fuzzy Adaptive Back-Stepping Sliding Mode Controller for High-Precision Deflection Control of the Magnetically Suspended Momentum Wheel. IEEE Trans Ind Electron 65:3530–3538. https://doi.org/10.1109/TIE.2017.2750617
46. Zhang M, Jing X (2021) A Bioinspired Dynamics-Based Adaptive Fuzzy SMC Method for Half-Car Active Suspension Systems With Input Dead Zones and Saturations. IEEE Trans Cybern 51:1743–1755. https://doi.org/10.1109/TCYB.2020.2972322
47. Lin B, Su X, Li X (2019) Fuzzy Sliding Mode Control for Active Suspension System with Proportional Differential Sliding Mode Observer. Asian J Control 21:264–276. https://doi.org/10.1002/asjc.1882
48. Hwang S, Kim HS (2020) Extended Disturbance Observer-Based Integral Sliding Mode Control for Nonlinear System via T–S Fuzzy Model. IEEE Access 8:116090–116105. https://doi.org/10.1109/ACCESS.2020.3004241
49. Ma X, Wong PK, Zhao J, Xie Z (2019) Cornering stability control for vehicles with active front steering system using T-S fuzzy based sliding mode control strategy. Mech Syst Signal Process 125:347–364. https://doi.org/10.1016/j.ymssp.2018.05.059
50. Xu K, Chen L, Lopes AM, et al (2023) Adaptive fuzzy variable fractional-order sliding mode vibration control of uncertain building structures. Eng Struct 282:115772. https://doi.org/10.1016/j.engstruct.2023.115772
51. Qiu Z, Zhang S (2016) Fuzzy fast terminal sliding mode vibration control of a two-connected flexible plate using laser sensors. J Sound Vib 380:51–77. https://doi.org/10.1016/j.jsv.2016.06.002
52. Oveisi A, Nestorović T (2016) Robust observer-based adaptive fuzzy sliding mode controller. Mech Syst Signal Process 76–77:58–71. https://doi.org/10.1016/j.ymssp.2016.01.015
53. Fang Y, Fei J, Hu T (2018) Adaptive backstepping fuzzy sliding mode vibration control of flexible structure. J Low Freq Noise, Vib Act Control 37:1079–1096. https://doi.org/10.1177/1461348418767097

54. Tang Z, Zhang T (2023) A hybrid control combining an advanced sliding mode control law with a proportional-derivative control by applying on vibration suppression. Mech Syst Signal Process 204:110771. https://doi.org/10.1016/j.ymssp.2023.110771
55. Yonezawa H, Yonezawa A, Kajiwara I (2025) Experimental verification of model-free active damping system based on virtual controlled object and fuzzy sliding mode control. Mech Syst Signal Process 224:111961. https://doi.org/10.1016/j.ymssp.2024.111961
56. Xinghuo Yu, Kaynak O (2009) Sliding-Mode Control With Soft Computing: A Survey. IEEE Trans Ind Electron 56:3275–3285. https://doi.org/10.1109/TIE.2009.2027531
57. Lu B, Fang Y, Sun N (2018) Continuous Sliding Mode Control Strategy for a Class of Nonlinear Underactuated Systems. IEEE Trans Automat Contr 63:3471–3478. https://doi.org/10.1109/TAC.2018.2794885
58. Young KD, Utkin VI, Ozguner U (1999) A control engineer’s guide to sliding mode control. IEEE Trans Control Syst Technol 7:328–342. https://doi.org/10.1109/87.761053
59. Alli H, Yakut O (2005) Fuzzy sliding-mode control of structures. Eng Struct 27:277–284. https://doi.org/10.1016/j.engstruct.2004.10.007
60. Jang JSR, Sun CT (1995) Neuro-Fuzzy Modeling and Control. Proc IEEE 83:378–406. https://doi.org/10.1109/5.364486
61. Lee H, Utkin VI (2007) Chattering suppression methods in sliding mode control systems. Annu Rev Control 31:179–188. https://doi.org/10.1016/j.arcontrol.2007.08.001
62. Sato Y, Yonezawa H, Yonezawa A, Kajiwara I (2022) Stability Improvement of Model-Free Control Based on a Virtual Structure Against the Resonance of a Proof-Mass Actuator. J Vib Eng Technol 10:1175–1188. https://doi.org/10.1007/s42417-022-00436-9
63. Yonezawa H, Kajiwara I, Yonezawa A (2019) Model-free vibration control to enable vibration suppression of arbitrary structures. In: 2019 12th Asian Control Conference, ASCC 2019. JSME, pp 289–294
64. Chilali M, Gahinet P (1996) H∞ design with pole placement constraints: An LMI approach. IEEE Trans Automat Contr 41:358–367. https://doi.org/10.1109/9.486637
65. Zhou K, Doyle JC, Glover K (1996) Robust and Optimal Control. PrenticeHall, New Jersey
66. Kajiwara I, Furuya K, Ishizuka S (2018) Experimental verification of a real-time tuning method of a model-based controller by perturbations to its poles. Mech Syst Signal Process 107:396–408. https://doi.org/10.1016/j.ymssp.2018.01.017

Figure captions:

Fig. 1: Proof-mass actuator.

Fig. 2: VCO-based model-free controller design: (a) real control system and (b) system with VCO.

Fig. 3: Transfer characteristic from vibration of the actual controlled object to that of VCO.

Fig. 4: Outline of the proposed control system.

Fig. 5: Triangular membership functions of the fuzzy sets: (a) switching function, (b) variation of the switching function, and (c) control effort.

Fig. 6: Configurations of controlled objects: (a) cantilever plate (Controlled object 1) and (b) both-ends-supported plate (Controlled object 2). The location where the blocks are attached as weights are indicated by broken lines.

Fig. 7: Time responses of the acceleration and control input in simulation for the cantilever plate (Controlled object 1).

Fig. 8: Time responses of the acceleration and control input in simulation for the both-ends-supported plate (Controlled object 2).

Fig. 9: Configurations of controlled objects: (a) Controlled object 3 and (b) Controlled object 4.

Fig. 10: Frequency response of the fixed 2DOF system (i.e., time-invariant system).

Fig. 11: Time histories of the performance index values with Controlled object 3.

Fig. 12: Time responses of the acceleration and control input with Controlled object 3.

Fig. 13: Time histories of the performance index values with Controlled object 4.

Fig. 14: Time responses of the acceleration and control input with Controlled object 4.